Chapter

21 Where Are We Going Now?

21.1 Introduction

To quote the old human rights song, we've come a long, long way – both since the genesis of modern MRI and since the start of the book. We started with an allusion to rocket science. In this last chapter we delve into what may have been regarded as science fiction, or mere star-gazing, a few years ago. What will tomorrow's MR scanner be like, and what will it do – or possibly, what won't it do? In the last edition we predicted:

- The use of interventional MRI will increase and expand, coupled with a proliferation of minimally invasive therapies, including gene therapies. *These are still on the way.*
- Interventional MR systems may use high-temperature superconducting flat magnets (like fridge magnets) incorporated into the operating room couch. *We're not there yet.*
- For screening we may see walk-through magnets. *Ha ha! We were probably watching Star Trek!*
- New extensions to parallel imaging will render EPI unnecessary except in some functional neurological examinations (i.e. just like the present!). *No comment.*
- Field strengths will of course keep increasing, and 3 T will become the norm for state-of-the-art clinical scanning. *This part is true.*
- There will be new 'intelligent' contrast agents for molecular-specific proton imaging. *Keep watching this space . . .*
- Finally, spectroscopy will be deployed as a routine clinical application. *Hooray, we got this one right too!*

21.2 7 Tesla Systems

In the last edition of this book we predicted (cautiously) that 'Field strengths will of course keep increasing, and 3 T will become the norm for state-of-the-art clinical scanning.' By 2014 the second part of this prediction was certainly true. By solving specific 3 T issues related to B_1 homogeneity, 3 T systems are able to provide high-quality images for all clinical applications, and they are economically within reach for most healthcare institutions. What about the first part, that field strengths will keep increasing? Well certainly, the first 7 T whole-body scanner was developed at the University of Minnesota in 1999 for research purposes; by 2003, all three major manufacturers launched their own 7 T systems to meet the growing demand from research centres around the world. The logical extension of clinical MRI from 3 T to 7 T has not yet happened – and may take several more years, for technical reasons that we will explain below.

The obvious attraction of going to 7 T is the improved SNR – just like the shift from 1.5 T to 3 T in the late 1990s. As we already saw, SNR scales approximately with B_0, so 7 T systems offer slightly more than double the SNR of a clinical 3 T system. The extra SNR is typically traded for much higher resolution. There are other differences of course: T_2s become shorter, and T_1s longer (see Table 21.1). SAR (specific absorption rate) also increases with B_0^2; together with the long T_1s, this means longer TRs and therefore longer scan times.

Of course, there are also disadvantages with going to higher field (apart from the costs). Due to the shorter wavelength, standing waves cause severe B_1 inhomogeneity even in small FOVs used for brain imaging, and the centre of the brain is often significantly brighter than the cortex (see Section 10.4.2). Overall image quality for clinical diagnosis is barely equal to the image quality available at 3 T. To overcome this, 7 T systems require multi-transmit coils and RF chains, probably with eight channels. Although the multi-transmit problem is 'solved' for 3 T, the extra work to develop eight-channel transmit systems, with the necessary safety controls, is

Table 21.1 Brain relaxation times at three field strengths

Tissue	T_1 (ms)[a]			T_2 (ms)[b]		
	1.5 T	3 T	7 T	1.5 T	3 T	7 T
White matter	646	838	1126	72	62	37
Grey matter	1197	1607	1939	90	71	43

[a] Wright PJ, Mougin OE, Totman JJ, *et al.* (2008) 'Water proton T1 measurements in brain tissue at 7, 3, and 1.5T using IR-EPI, IR-TSE, and MPRAGE: results and optimisation'. *Magn Reson Mater Phy* 21:121–130.
[b] Zhu J, Klarhofer M, Santini F, *et al.* (2014) 'Relaxation measurements in brain tissue at field strengths between 0.35T and 9.4T'. *Proc Intl Soc Mag Reson Med* 22:3208.

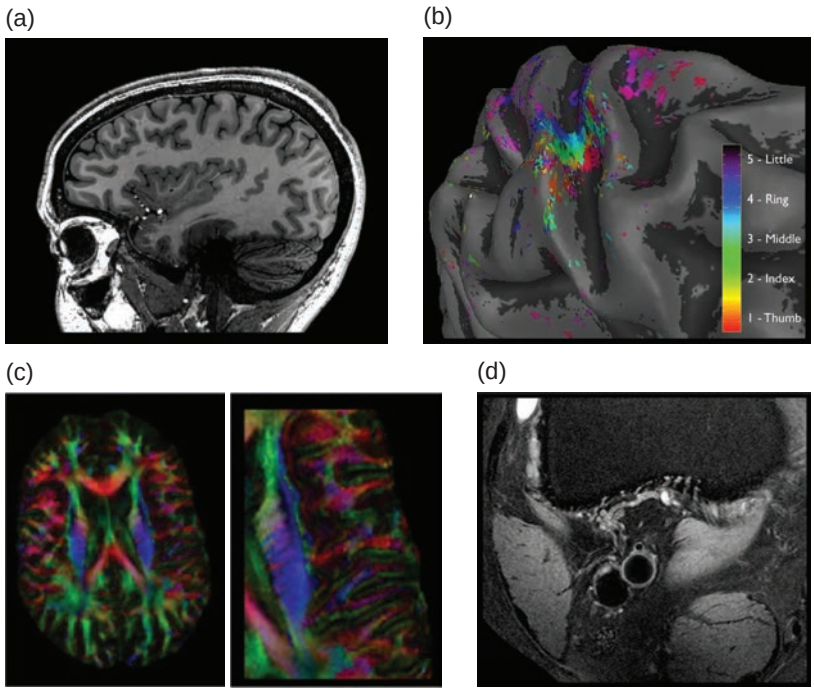

Figure 21.1 7 T imaging often uses the higher SNR to achieve much higher spatial resolution than clinical systems. (a) MP-RAGE with 0.6 mm isotropic voxels (courtesy of Utrecht Medical Centre, Netherlands); (b) finger-tapping fMRI with high resolution, distinguishing between individual digits (courtesy of Sir Peter Mansfield MRI Centre, Nottingham, UK); (c) high-resolution FA map (courtesy of Vanderbilt University, Nashville TN); (d) popliteal artery wall imaging (courtesy of Utrecht Medical Centre, Netherlands).

significant. The very high SAR deposition at 7 T is extremely limiting for standard pulse sequences. For example, TSE T_2w or T_1w scans with even a modest train of refocusing pulses requires a long TR to keep SAR under control, which leads to very long scan times to achieve whole-brain coverage. Therefore many 7 T scans are done using gradient echo.

Susceptibility effects also become very challenging at 7 T, and systems require extra B_0 shimming. The shimming involves not only first- and second-order shim coils, but also third order; these extra shim coils take up more space in the magnet bore, so the internal patient aperture is usually 55–60 cm, instead of the more usual 70 cm in a clinical system. The susceptibility effect can also be an advantage, however, particularly for detection of the BOLD effect in fMRI. One of the main applications for 7 T scanning is high-resolution fMRI which can localize brain function with very high spatial resolution.

Today (early 2015) there are approximately 60 installations of 7 T MR systems worldwide. There is still significant development work to do to make these systems clinically useful and to improve diagnostic abilities. We need a wider range of RF receive coils, as well as the multi-transmit capabilities, and we need to guarantee safety, e.g. by developing special

low-SAR excitation and refocusing RF pulses. Will 7 T become clinically relevant in the next decade? These authors are not ready to place their bets, yet.

21.3 Hyperpolarization

Polarization in MRI refers to the number of excess nuclei in the low-energy state that contribute to the net or bulk magnetization. The polarization at thermal equilibrium for a spin ½ nuclei is given by (see Box 'Population of Energy States' in Section 9.3)

$$P \approx 1 - \frac{\gamma \hbar B_0}{k_B T}$$

Hence P is approximately 5×10^{-6} at 1.5 T for ^{1}H which is at 80 M concentration in biological tissues. However, other NMR active nuclei that we may be interested in have either very low natural abundance, e.g. ^{13}C, or are not naturally occurring in the body, e.g. noble gases such as ^{129}Xe. The theoretically achievable SNR for a given nucleus is proportional to $C\gamma P$, where C is the concentration, γ is the gyromagnetic ratio and P is the polarization. Since we cannot increase C substantially and γ is a constant, the only option is to try to increase the polarization P. Increasing the static magnetic field strength B_0 is one way to increase the polarization, but also has a number of drawbacks, not least of which is cost. An alternative, and completely different, approach is to create an artificial, non-equilibrium distribution of the nuclei known as the 'hyperpolarized' state, which creates a several orders of magnitude increase in polarization. This hyperpolarized state is most effectively created by an external polarization of a suitable substrate, followed by rapid administration of the hyperpolarized agent. For example, hyperpolarization of noble gases such as ^{129}Xe or ^{3}He can be achieved using optical pumping while hyperpolarization of a wide range of organic molecules containing ^{13}C can be achieved using either parahydrogen-induced polarization (PHIP) or dynamic nuclear polarization (DNP).

In DNP the ^{13}C is hyperpolarized by transferring spin polarization from electrons to protons. This phenomenon was theoretically predicted by Albert Overhauser in 1953 and relies on the random interactions between an electron and a nucleus. The ^{13}C agent to be polarized is mixed with an organic radical with unpaired electrons, which is known as the electron paramagnetic agent (EPA). The sample is then placed in a polarizer which keeps it at a very low temperature, <1 K, in a high magnetic field, typically 5 T. At these extreme physical conditions the EPA electrons are nearly 100% polarized. The sample is then irradiated with microwave energy at a frequency corresponding to the electron spin resonance of the EPA at that field strength. This transfers the polarization from the electrons to the ^{13}C nuclei. The polarization builds up over a period of 15–60 min, after which time the frozen sample is dissolved in heated water or buffer to produce a room-temperature solution, a process known as dissolution. Typically hyperpolarization with DNP can result in a more than 10 000-fold increase in SNR, making it possible to monitor real-time changes in metabolism.

Hyperpolarized nuclei have the advantage that they are either not naturally present in the body, such as ^{129}Xe or ^{3}He, or they have very small natural abundance, such as ^{13}C. The low background signal produces high levels of image contrast. The disadvantage is that separate transmit and receive coils tuned to the precessional frequency of the nuclei at the field strength of interest are required. Similarly larger gradient amplitudes are required for equivalent spatial resolution to proton imaging since the slice thickness and pixel sizes are all scaled by γ. The resolution of hyperpolarized imaging is therefore generally inferior to proton imaging. The hyperpolarization signal of most biological molecules decays with a T_1 of the order of a few tens of seconds, so it is critical to inject and image the agent as rapidly as possible after dissolution and to use a low flip angle imaging sequence to avoid consuming the hyperpolarized magnetization too quickly.

Hyperpolarized gases such as ^{129}Xe or ^{3}He have been used for imaging the lung since they can be readily inhaled by the patient and provide direct visualization of the airspaces (Figure 21.2). As such they are both suited to 'ventilation' imaging, i.e. demonstrating that the gas can reach the lung alveoli. This is important in monitoring diseases such as chronic obstructive pulmonary disease, cystic fibrosis and asthma. The self-diffusion (ADC) of the gases can also be measured to aid in the assessment of airway size, which can change due to diseases such as emphysema. In addition ^{129}Xe is also slightly soluble in tissue and blood, which means it can also be used for investigating diseases that impair the exchange of gas across the alveolar wall, e.g. fibrosis or certain interstitial lung diseases.

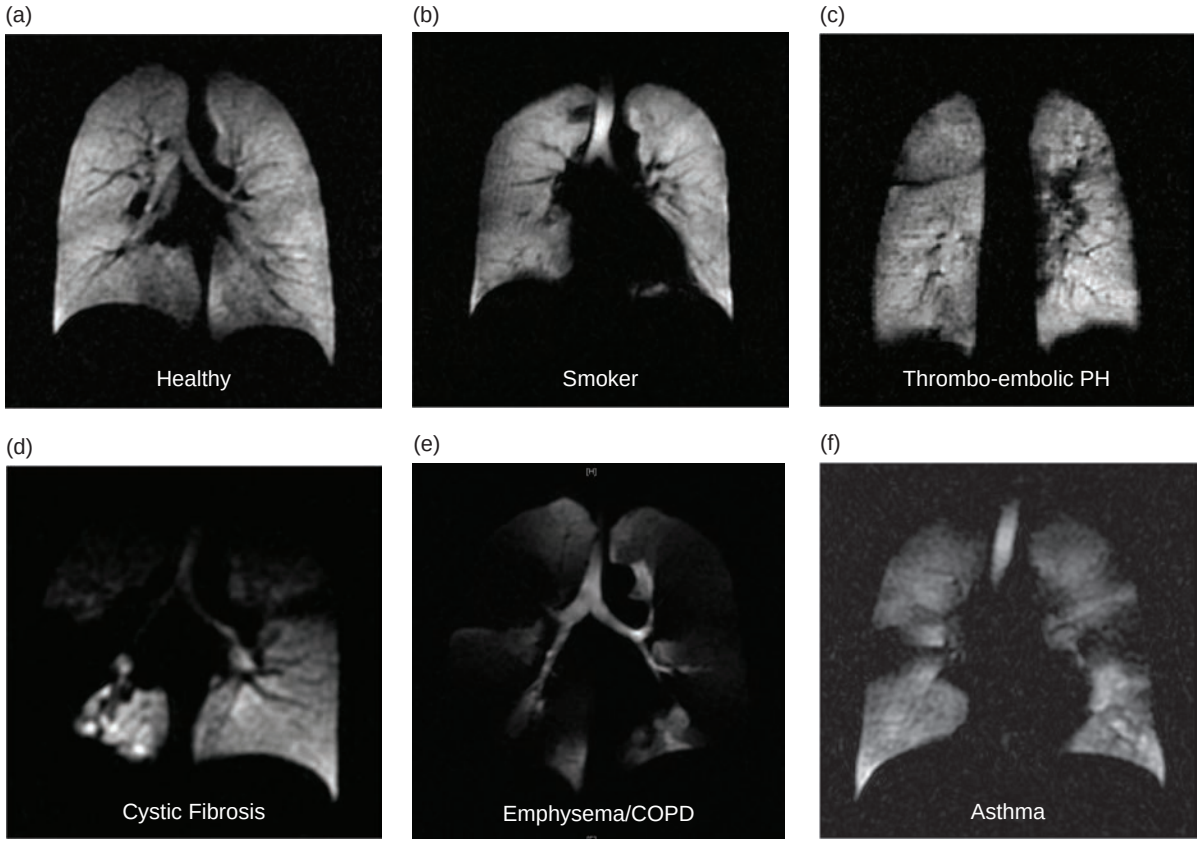

Figure 21.2 Hyperpolarized ^{3}He ventilation images acquired at breath-hold from subjects with different obstructive airway diseases. Courtesy of Prot. Jim Wild, University of Sheffield, UK.

Hyperpolarized ^{13}C Using DNP

Hyperpolarized ^{13}C is of particular interest for characterizing tumour metabolism. Malignant cancer cells have a metabolism some 200 times greater than normal cells, which is demonstrated by the high uptake of a radioactive form of glucose in **P**ositron **E**mission **T**omography (PET) imaging. In normal tissue, in the presence of oxygen, glucose is converted into pyruvate which in turn is metabolized in the tricarboxylic acid cycle (TCA) to produce ATP, the molecule that supplies energy for cell metabolism. This is a process known as oxidative phosphorylation. Without oxygen, pyruvate is converted to lactate in a process known as anaerobic, i.e. without oxygen, glycolysis catalysed by the enzyme lactate dehydrogenase (LDH). However, in cancer cells aerobic glycolysis occurs, i.e. the majority of the pyruvate is converted into lactate even in the presence of oxygen. This is known as the Warburg effect. This conversion of glucose into lactate can be decreased in tumours undergoing cell death induced by chemotherapy.

The only hyperpolarized ^{13}C human study to date has used ^{13}C-labelled pyruvate which has a sufficiently long T_1 (approx. 30 s) to demonstrate elevated [1–^{13}C]lactate/[1–^{13}C]pyruvate ratios in regions of biopsy-proven prostate cancer. Although used in a number of animal studies, the paucity of clinical studies is due to the challenges in producing a sterile hyperpolarized agent such as [1–^{13}C]pyruvate that can be injected into patients. This first human study required a 'clean-room' adjacent to the MRI system in order to prepare the sterile fluid paths (SFP) containing the sample and then to rapidly quality control (QC) the agent between dissolution and injection. Recently a standalone DNP polarizer, designed for

sterile use, has become commercially available. Although the single-use SFP requires filling in a clean environment, afterwards it can be stored at –20 °C (to keep the pyruvate frozen) prior to insertion into the polarizer. Once polarized the system also provides a non-contact QC system. The system automatically fills a standard power injector syringe which is then quickly passed into the magnet room and injected into the subject.

21.4 MR-PET

Combined MR-PET is a natural extension of the wide commercial availability of PET-CT. There is, however, a number of challenges and opportunities associated with MR-PET. The main issue is the PET detector assembly. In a PET-CT 511 keV γ-ray photons hit an inorganic scintillation crystal which creates tens of thousands of optical photons, a flash of light known as a 'scintillation'. The scintillation crystal is coupled to a photo-detector, typically a photomultiplier tube (PMT) that converts the scintillation to an electrical current. In a PMT the optical photons strike a photocathode surface that releases a small number of electrons. These are then accelerated within a vacuum tube, hitting further electrodes (dynodes) that release more electrons, causing a massive cascade. After several dynode stages a large number of electrons hit the anode, resulting in a measurable current pulse. Unfortunately PMTs are very sensitive to magnetic fields. One manufacturer's approach is to have a physical separation between the MRI magnet and the PET detector ring containing the PMTs. The common patient table can be directly moved out of the MRI scanner and into the PET detector, allowing for sequential imaging. Other manufacturers have opted for systems whereby the PET detector is positioned inside the MRI magnet for true simultaneous PET-MR (see Figure 21.3). This has required the development of magnetic field insensitive photo-detectors. The most widely used technology is that of the Avalanche Photo Diode (APD) which is essentially a semiconductor version of a PMT, although it has a much lower gain. More recently silicon photomultipliers have been developed which are essentially many APDs connected in parallel, resulting in a higher sensitivity and response speed.

A further challenge in PET-MR is the attenuation correction. PET works by coincidence detection of two γ-rays being produced 180° apart when an electron annihilates with a positron. Attenuation is when the two coincidence events do not get recorded within a very short period of each other due to either γ-ray getting absorbed in the body or scattering outside the detector FOV. This loss of photons increases the noise in the PET image as well as causing artefacts and distortions. The attenuation of photons can be corrected if the tissue density is known. In PET-CT the CT not only provides a high-resolution anatomic image, onto which the lower-resolution PET image can be overlaid, but it also provides a direct measurement of tissue radiodensity, i.e. the Hounsfield scale. The signal intensity in MRI, of course, has nothing to do with tissue radio-density, hence an active area of development for PET-MR is in deriving attenuation correction maps from MRI data. The main approaches to date have been to use different pulse sequences, e.g. Dixon techniques, to identify different tissues such as fat, water, lung and air and then assign them appropriate attenuation coefficients. Bone has a very high attenuation and some groups have attempted to register the MR data to CT bone atlases to derive a pseudo-CT for each patient. Ultra-short TE (UTE) sequences have been used in an attempt to identify bone directly from MR images. As well as

Figure 21.3 PET-MRI system: the Siemens mMR Biograph with cutaway to show the PET detector ring. Courtesy of Siemens Healthcare.

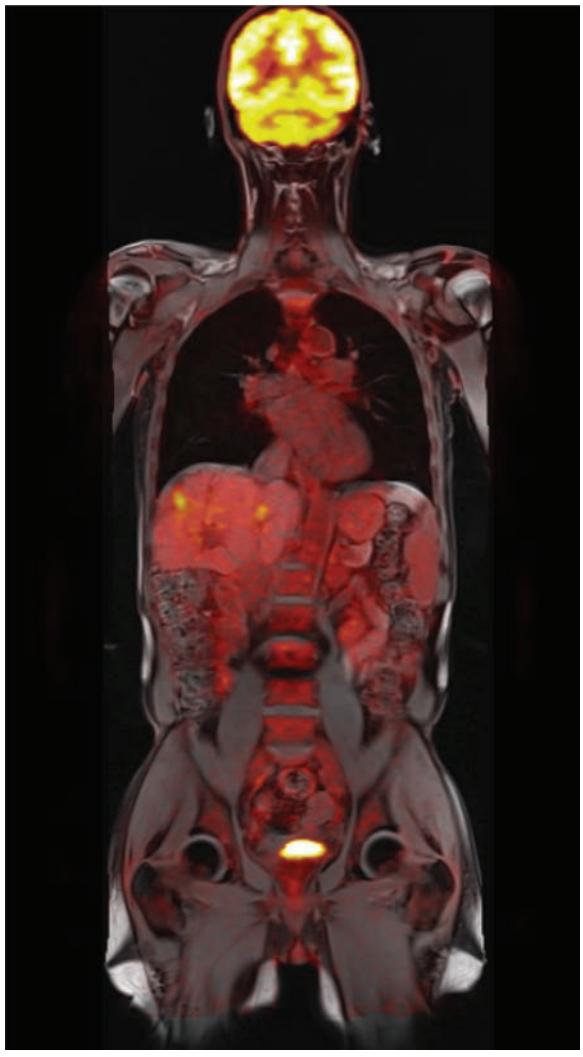

Figure 21.4 PET-MRI: ^{18}F-FDG injected dose 370 MBq, uptake time 60 min, overlaid on T_1 fat sat coronal showing established liver disease with multi-focal areas of increased FDG uptake along intrahepatic biliary ducts. Courtesy of Dr Anna Barnes, University College Hospital, London.

tissue attenuation it is also necessary to account for the attenuation caused by the RF coils and other high-density materials, e.g. the patient table. Rigid structures, like head coils, whose position is fixed in the scanner bore, can be imaged using CT and the attenuation maps incorporated into the patient-specific maps. Flexible coils that can be freely positioned present additional challenges in identifying their location. Again UTE sequences may help to identify coil structure in the FOV.

Finally patients in PET-CT are usually scanned with their arms above their head so that the arms do not contribute to the tissue attenuation. The reduced bore size in PET-MR means that this is not generally possible. If the arms are not fully covered in the MR field-of-view then the attenuation maps may be incomplete: this is known as truncation artefact and the manufacturers have developed various methods to try to address this problem.

21.5 MR-LINAC

Conformal radiotherapy (RT) relies upon accurate 3D localization of the cancer and surrounding healthy tissue. Currently CT is the modality of choice for RT planning as it provides 3D images and information on the electron density required for accurate radiation dosimetry. However, its discrimination of soft tissue is inferior to MRI and, while fast, lacks some of the latter's advanced motion correction options such as navigator echoes. Internal organ motion, mainly from respiration, is a major problem in RT, as a larger volume of tissue has to be treated to ensure that the treatment area is fully covered. MRI's superior soft tissue information and motion correction options could enable a reduction in the treatment volume, thus sparing adjacent healthy tissue. Further benefit may derive from the ability to utilize advanced MR techniques to plan and monitor the response to treatment in real time.

The challenges of combining a Linear Accelerator (Linac) with an MRI scanner are significant, given the requirement for the fine control of high-energy (6 MeV) electron beams for accurate treatment. These are accelerated using microwave technology and then bent and field-shaped magnetically. Usually a Linac would be sited in a region of very low (earth's) magnetic field (see Table 2.1), so considerable modifications are required in order for it to operate in the region of the scanner's field! One feasible design is to use a split bore magnet, with the Linac mounted in the gap (see Figure 21.5), while in another, the Linac is mounted on the magnet axis. Some designs even have a rotating patient couch. Other challenges for the MR component are similar to those encountered in PET-MR – a need to be able to account for the attenuation of the tabletop and coils. Ultra-short TE (UTE) imaging may be useful in this respect and also in its ability to image bone directly.

At the time of writing a number of prototype systems are in existence and are currently undergoing pre-clinical commissioning.

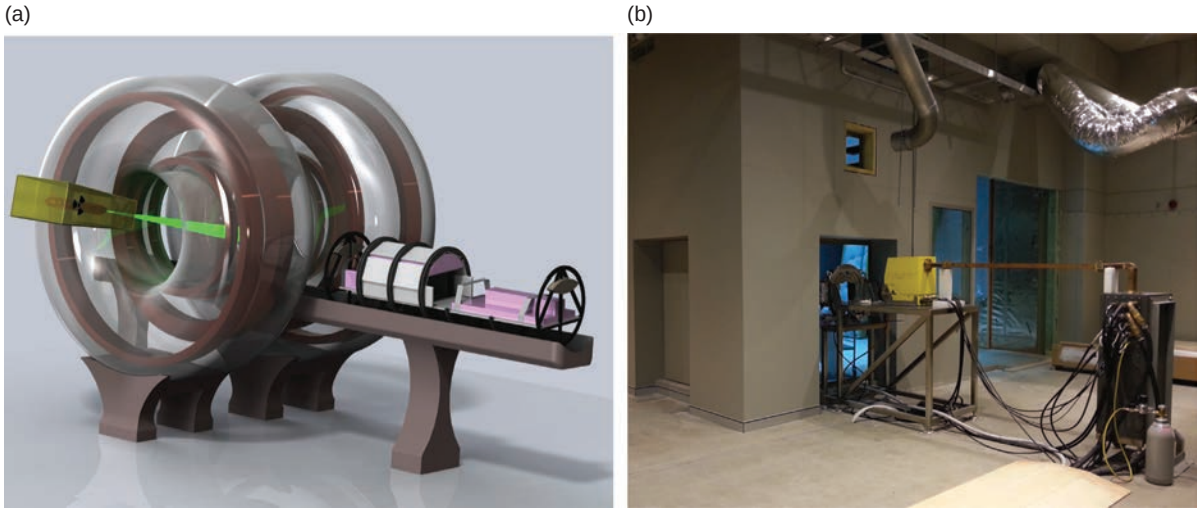

Figure 21.5 (a) Artist's impression of MR Linac; (b) the actual Linac bunker. Courtesy of Gary Liney and Brendan Whelan as part of the Australian MR-Linac program.

Further Reading

Feinberg DA and Yacoub E (2012) 'The rapid development of high speed, resolution and precision in fMRI'. *Neuroimage* 62:720–725.

Kauczor H-U (ed.) (2000) 'Special issue: hyperpolarised gases in MRI'. *NMR Biomed* 13(4):173–264.

Stafford RJ (2004) 'High field MRI: technology, applications, safety, and limitations'. American Association of Physicists in Medicine, 46th Annual meeting. Available from www.aapm.org/meetings/04AM/pdf/14–2351-12342.pdf [accessed 8 May 2015].